

Pd–Sn/Al₂O₃ catalysts from colloidal oxide synthesis

I. Preparation of the catalysts

S. Verdier,^a B. Didillon,^b S. Morin,^c J.C. Jumas,^d J. Olivier-Fourcade,^d and D. Uzio^{c,*}

^a Rhodia, CRA 52, rue de la Haie Coq, 93308 Aubervilliers Cedex, France

^b Rhodia, CRL 85, rue des Frères Perret, 69192 St-Fons Cedex, France

^c IFP, 1-4 avenue de Bois Préau 92852, Rueil-Malmaison Cedex, France

^d LAMMI, UMR 5072, Université Montpellier II, CC 015, Place E. Bataillon, 35095 Montpellier Cedex 5, France

Received 9 October 2002; revised 23 January 2003; accepted 10 February 2003

Abstract

Colloidal oxide synthesis is a new technique for the preparation of bimetallic supported particles which provides the opportunity to control particle size distribution and interaction between both metals. It consists in synthesizing in aqueous medium a sol of colloidal oxide Pd–Sn nanoparticles which is further deposited onto a porous support. In this work, this method has been applied to the preparation of Pd–Sn/Al₂O₃ dedicated to the selective hydrogenation of unsaturated hydrocarbons. Two synthesis routes, *surface precipitation* and *surface adsorption*, are described to demonstrate the potential of colloidal oxide chemistry to generate a bimetallic interaction in aqueous solution which is strengthened during the reduction step after deposition onto alumina. ¹¹⁹Sn Mössbauer spectroscopy (¹¹⁹Sn MS) and transmission electron microscopy (TEM) were used to characterize the sols and the supported catalysts. This allowed us to determine the key parameters of colloidal oxide synthesis as far as formation of bimetallic Pd_xSn_y phases is concerned.

© 2003 Elsevier Inc. All rights reserved.

Keywords: Bimetallic; Palladium; Tin; Colloidal synthesis; Selective hydrogenation; ¹¹⁹Sn Mössbauer spectroscopy

1. Introduction

The control of the properties of bimetallic particles is a key point for studies devoted to establishing the relationships between structure and reactivity. Indeed, catalysts with the same nominal composition may exhibit very different catalytic performance because of differences in the active sites at the nanometer scale. In order to control the characteristics of bimetallic supported catalysts, many interesting preparation methods have been investigated in the literature. For instance, controlled surface reactions such as redox or electrochemical methods [1] and techniques based on surface organometallic chemistry [2,3] have demonstrated their abilities to obtain well-designed bimetallic supported nanoparticles. Progress in vapodeposition techniques has recently shown promising improvement for depositing bimetallic aggregates with a monomodal particle size distribution and uniform composition [4].

Metallic colloidal synthesis has also been explored for the preparation of mono and bimetallic supported catalysts [5–9]. In this method, a metallic sol is first synthesized and further deposited onto a support to yield the metallic supported catalyst after a mild activation step. Colloidal mono or bimetallic particles are usually formed by condensation of the metallic precursors using various methods [10] such as photoreduction [11], radiolysis [12], or chemical reduction using an organic reducing agent [13–16]. Moreover, in order to prevent sols from aggregation, organic ligands or polymers are usually adsorbed on the metallic colloidal particles. As an example, poly(*N*-vinyl-2-pyrrolidone)-stabilized Pd-based sols modified by Pt [17], Au [18], Cu [19], or Ni [20] have been obtained by solvent reduction by Toshima et al. Their colloidal nanoparticles are characterized by a narrow particle size distribution (mean diameter < 2 nm) and controlled structures (alloy, core-shell, etc.).

Nevertheless, all those methods may have some specific features which make them difficult to extrapolate to an industrial scale like the use of organic precursors or solvents. For this purpose, aqueous medium remains the most suitable

* Corresponding author.

E-mail address: denis.uzio@ifp.fr (D. Uzio).

phase to prepare large quantities of catalysts. Moreover, dry impregnation and ion exchange followed by thermal activation, which have been widely used to manufacture bimetallic catalysts, have shown their limitations as far as a control of the particle size and composition at the nanometer scale is desired. This is particularly true in the case of large particles required for demanding reactions such as selective hydrogenation of polyunsaturated hydrocarbons. Indeed, the reactivity of the metallic precursors toward the oxide surface sites may be unfavorable to the bimetallic interaction if one of the metallic complexes has more affinity with the support than with the other metal.

The sol-gel route has been largely reported for the synthesis of a wide class of materials but the resources of this chemistry in the aqueous phase for the synthesis of bimetallic nanoparticles have not been exploited. Oxide colloidal route is a promising alternative to produce in aqueous solution well-designed bimetallic supported catalysts. Already applied to the case of monometallic Pd/Al₂O₃ system [21], this method consists in the synthesis of oxide colloidal nanoparticles in aqueous solution prior to the deposition on the support. Subsequent low thermal activation is sufficient because the oxide phase is already formed. This work is dedicated to the application of the oxide colloidal route to the synthesis of bimetallic Pd–Sn catalysts. In this paper, the experimental procedures are given in Section 2 and discussion concerning the influence of the preparation parameters on the final characteristics of the supported catalysts is in Section 3. Relationships between structure and catalytic properties in selective hydrogenation of buta-1,3-diene will be detailed in part II of the study [22].

2. Experimental

2.1. Catalysts synthesis

Two routes to colloidal oxide synthesis have been investigated in this paper: *surface precipitation* and *surface adsorption*.

In the first route called surface precipitation, palladium(II) is precipitated on the surface of colloidal particles of tin(IV) oxide SnO₂ by progressively adding 0.5 N soda till pH 8 to an equimolar solution ([Pd] = [Sn] = 4.2 × 10⁻² mol/L) of palladium nitrate (Pd(NO₃)₂ in nitric acid from Heraüs) and tin(IV) chloride (SnCl₄ · 5H₂O from Aldrich). The resulting sol is immediately wet impregnated onto a γ-Al₂O₃ (120 m²/g, beads from Axens) to yield the supported Pd–Sn catalyst which is called in the following SnO₂–PdO.

In the second route called surface adsorption, a stannate complex Sn(OH)₆²⁻ is adsorbed on the surface of colloidal nanoparticles of palladium oxide. The PdO nanoparticles are first synthesized by adding a solution of palladium nitrate ([Pd] = 3.2 × 10⁻² mol/L) into 0.5 N soda until pH 12.1. The synthesis and characterization of these PdO colloidal

particles, whose mean diameter is 1.8 nm, have been previously described [21]. A tin(IV) chloride solution ([Sn] = 8.4 × 10⁻² mol/L) is then added to the sol so that the molar ratio Pd/Sn is equal to 2. The pH after addition of tin(IV) to the PdO sol is 12.0. In the following, the resulting bimetallic sol will be referenced as the PdOSn sol. As in surface precipitation, γ-Al₂O₃ (120 m²/g, beads from Axens) is impregnated with the PdOSn hydrosol yielding the PdOSn catalyst. In this route, the influence of the sol preparation time has been studied. In the PdOSn1 catalyst, the sol is immediately deposited onto the support immediately after its preparation. But in the case of the PdOSn2 catalyst, the sol is agitated 75 min after preparation before impregnation of the alumina support. The corresponding sols are referenced as the catalysts.

In this work, all the catalysts are dried 12 h at 120 °C and further air calcined 2 h at 200 °C (5 °C/min). If necessary, they are reduced under hydrogen 2 h at a temperature between 200 and 400 °C (5 °C/min) before characterization or catalytic evaluation (reported in part II of this study [22]). The gas flow during these activation steps is set at 1 L/(h g_{catalyst}). The metal loadings of the bimetallic catalysts have been determined by atomic emission spectroscopy (AES-ICP) like the concentrations of sodium and chlorides.

2.2. Characterization techniques

2.2.1. Transmission electron microscopy (TEM)

TEM was carried out on a JEOL 2010 at 200 kV. Particle size distributions were obtained by measuring more than 100 particles on the micrographs of the 200 °C reduced catalysts.

2.2.2. ¹¹⁹Sn Mössbauer spectroscopy (¹¹⁹Sn MS)

¹¹⁹Sn Mössbauer spectroscopy experiments were carried out at the LAMMI (Montpellier) at room temperature using an EG & G Novelec constant acceleration spectrometer in transmission mode. The source of γ-rays was ^{119m}Sn in a BaSnO₃ matrix with a nominal activity of 10 mCi. The velocity scale was calibrated using the magnetic sextet of a high-purity iron foil absorber as a standard, with ⁵⁷Co(Rh) as the source. All the spectra were analyzed by fitting the recorded spectra to Lorentzian profiles by the least-squares method using the ISO software [23]. Goodness of fits was controlled by the classical X² test. All isomer shifts are given relative to the center of the BaSnO₃ spectrum recorded at room temperature. The relative proportions of all different species can be roughly estimated from their relative contribution to the total spectral absorption, provided that the probabilities for recoilless resonant absorption of γ radiation are known for each individual species. These probabilities, expressed by the Lamb–Mössbauer factor *f*, depend strongly on the lattice type and the bonding properties. The exact values of the *f* factors for the various species described here are unknown and are therefore supposed to be identical. This simplification induces a small error which is estimated to be approximately 10%. The absorbers were pre-

pared from 2.5 g of catalyst in specific Pyrex cells which can be sealed under controlled atmosphere in order to avoid any exposure to air and then transferred into the spectrometer. For the study of the $\text{Sn}(\text{OH})_6^{2-}$ solution and the PdOSn1 sol, 2 cm² of blotting paper has been impregnated with 2 ml of these solutions and then cooled to -193°C in a cryostat before recording the spectra. The $\text{Sn}(\text{OH})_6^{2-}$ solution ($[\text{Sn}] = 1.3 \times 10^{-2}$ mol/L) has been prepared by dissolution of $\text{SnCl}_4 \cdot 5\text{H}_2\text{O}$ in 1 M soda. The PdOSn1 sol is frozen immediately after preparation.

3. Results and discussion

The main characteristics of the different catalysts prepared via surface precipitation and surface adsorption are summarized in Table 1.




For all the catalysts, both Pd and Sn are located in the periphery of the beads in a narrow shell of about 150 μm thickness as shown by Castaing Microprobe analysis (not

presented here). Moreover, analysis of the different catalysts by X-ray diffraction did not allow us to observe X-ray patterns relative to the alumina-supported metallic phase.

3.1. Surface precipitation route

In this route, an acidic bimetallic solution of $\text{Pd}(\text{NO}_3)_2$ and $\text{SnCl}_4 \cdot 5\text{H}_2\text{O}$ is progressively neutralized by 0.5 N soda. The UV–vis spectrum of the starting Pd–Sn solution displays an absorption band at 427 nm which can be assigned to $\text{PdCl}_3(\text{H}_2\text{O})^-$ or $\text{PdCl}_2(\text{H}_2\text{O})_2$ complexes [24]. This result indicates that chlorides originating from the stannic salt $\text{SnCl}_4 \cdot 5\text{H}_2\text{O}$ preferentially coordinate with palladium. As complexation of palladium with chlorides decreases its acidity [25], the palladium complex is neutralized after the tin(IV) complex in the bimetallic solution as illustrated in Fig. 1. Until point A, both free protons and tin(IV) are neutralized whereas palladium reacts with hydroxide anions between points A and B.

Table 1
Main characteristics of the different catalysts

	$\text{SnO}_2\text{-PdO}$	PdOSn1	PdOSn2
Method	Surface precipitation 	Surface adsorption 	Surface adsorption 
Preparation time (min)	15	15	90
Pd (wt%)	0.30	0.30	0.30
Sn (wt%)	0.33	0.17	0.17
Molar Pd/Sn	1	2	2
Na (wt%)	0.50	0.70	0.70
Cl (wt%)	0.40	0.20	0.20

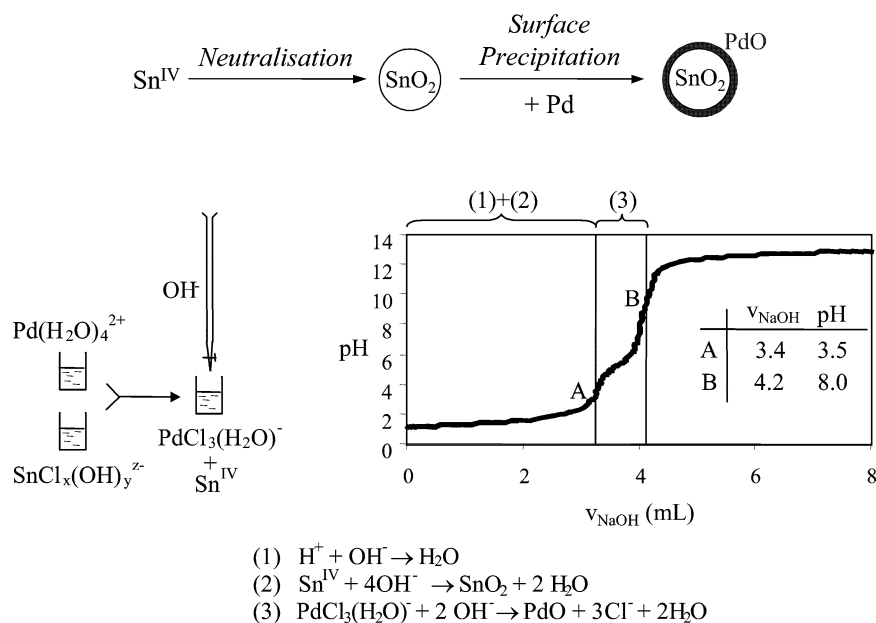


Fig. 1. Neutralization curve by 0.5 N soda of a bimetallic solution of $\text{Pd}^{\text{II}}\text{-Sn}^{\text{IV}}$: 5 mL $\text{Pd}(\text{NO}_3)_2$ in HNO_3 0.165 N + 5 mL $\text{SnCl}_4 \cdot 5\text{H}_2\text{O}$ in H_2O ($[\text{Sn}] = [\text{Pd}] = 4.2 \times 10^{-2}$ mol/L).

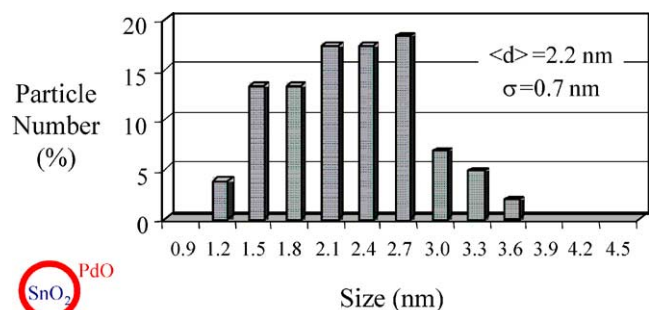


Fig. 2. Particle size distribution of SnO_2 -PdO catalysts measured by TEM.

The colloidal solution obtained at point B (see Fig. 1), i.e., when tin(IV) and Pd(II) have been subsequently neutralized in this order, is then impregnated in the porosity of the γ - Al_2O_3 beads. The resulting SnO_2 -PdO catalyst has been then characterized by TEM and Mössbauer spectroscopy.

Fig. 2 displays the particle size distribution obtained by TEM analysis for the SnO_2 -PdO catalyst. A rather narrow distribution is observed centered on 2.2 nm average diameter. Micrographs also show the presence of some aggregated particles between 50 and 200 nm in size. When compared to the size distributions of SnO_2 (mean diameter = 2.0 nm) and PdO (mean diameter = 1.8 nm) nanoparticles prepared using the same route, such a result is consistent with the formation of a PdO coating onto SnO_2 nanoparticles. Indeed, considering the mean size of SnO_2 particles and the molar Pd/Sn ratio, surface precipitation of PdO onto SnO_2 would only concern a few atomic layers-of PdO and therefore would slightly increase the mean diameter of the starting particles. Moreover, heterogeneous nucleation is expected to occur due to more favorable energetic pathways when compared to homogeneous nucleation. Coatings of hematite α - Fe_2O_3 or TiO_2 particles with different metallic oxides have been reported in the literature using similar synthesis routes [26–28]. However, at this point, the formation of PdO and SnO_2 nanoparticles with no interaction can be completely ruled out.

Regarding the interaction between palladium and tin, ^{119}Sn Mössbauer spectroscopy is a powerful technique giving access to the variation of the oxidation state, environment, and electronic effect relative to Sn. Spectra relative to

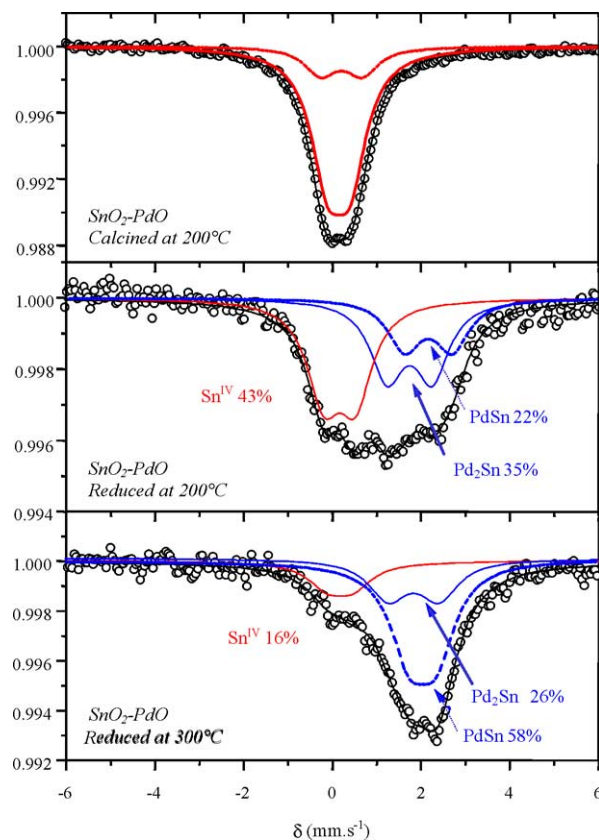


Fig. 3. ^{119}Sn Mössbauer spectra of the SnO_2 -PdO catalyst calcined at 200 °C (top) and further reduced at 200 °C (middle) and 300 °C (bottom).

the SnO_2 -PdO catalyst are presented in Fig. 3 and the different Mössbauer parameters are reported in Table 2. After air calcination, the isomer shift δ is about 0.04–0.09 mm/s, indicating the presence of stannic tin. Upon reduction with hydrogen, tin progressively incorporates into palladium to form bimetallic phases Pd_xSn_y : PdSn, the expected one (Pd/Sn = 1), but also Pd_2Sn . The composition of these phases has been estimated from the values of isomer shifts of bulk Pd–Sn alloys or intermetallics [29] which are linearly dependent with the tin proportion [30,31] and by comparison with recent Mössbauer studies on Pd–Sn catalysts [32,33]. It is remarkable to note that 57% of tin is in the metallic state after reduction at 200 °C whereas tin remains in the +IV

Table 2

Hyperfine parameters of refined spectra of the SnO_2 -PdO catalyst after calcination and reduction: isomer shift (δ) relative to BaSnO_3 , quadrupole splitting (Δ), full width at half-maximum (Γ), and relative contribution (RC)

Sample	δ (mm/s)	Δ (mm/s)	Γ (mm/s)	RC (%)	Sn species
SnO_2 -PdO calcined at 200 °C	0.04 (1)	0.51 (2)	0.88 (2)	81	Sn^{IV} type1
	0.09 (4)	0.95 (7)	0.9 (1)	19	Sn^{IV} type2
SnO_2 -PdO reduced at 200 °C	0.06 (3)	0.71 (3)	0.92 (5)	43	Sn^{IV} type1
	1.63 (5)	1.02 (3)	0.92 (5)	35	$\text{Pd}_2\text{Sn}^{\text{a}}$
	2.05 (6)	1.08 (4)	0.92 (5)	22	PdSn^{a}
SnO_2 -PdO reduced at 300 °C	0.06 (4)	0.59 (7)	1.05 (5)	16	Sn^{IV} type1
	1.74 (3)	1.15 (5)	1.05 (5)	26	$\text{Pd}_2\text{Sn}^{\text{a}}$
	1.94 (1)	0.61 (3)	1.05 (5)	58	PdSn^{a}

^a After the parameters reported for Pd–Sn bulk alloys and intermetallics in [29].

oxidation state under the same conditions in an alumina-supported tin catalyst prepared as SnO₂–PdO but without palladium. After reduction at 300 °C, the amount of reduced tin alloyed with palladium reaches 84% which is a clear indication of the initial strong interaction existing in the oxidized state between the two elements. Interestingly, among the two forms of stannic species observed after calcination, the second one, Sn^{IV} type 2, disappears upon reduction. Being characterized by a high Δ value consistent with a distorted local environment of tin, this species could be attributed to tin in very close interaction with palladium. Even more interestingly, almost all the palladium is alloyed with tin after reduction: 92% ($35 \times 2 + 22 = 92$) at 200 °C and 100% ($26 \times 2 + 58 = 110$) at 300 °C. Alumina-supported tin is known to be hardly reduced at the metallic state because, among others, of the formation of tin aluminate species [34]. This is what is usually observed with conventional preparation methods such as impregnation [32]. In the case of the SnO₂–PdO catalyst prepared by surface precipitation in the oxide colloidal synthesis, the formation of Pd–Sn alloyed phases is strongly favored, indicating that an intimate interaction between Sn and Pd has been set in the sol consistent with precipitation of PdO onto colloidal SnO₂ particles.

3.2. Surface adsorption route

In this route, a stannic complex is contacted with an alkaline hydrosol of 1.8 nm particles of PdO. After the addition of the tin(IV) chloride solution to the PdO sol, the starting pH 12.1 is slightly decreased to pH 12.0. Under these conditions, chlorides are substituted in the coordination sphere of tin(IV) by hydroxo anions which are in large excess yielding the stannate Sn(OH)₆²⁻ complex. In the following, the PdO sol added with Sn(OH)₆²⁻ anions will be referenced as the PdOSn sol. Immediately after its preparation, the bimetallic sol, referenced as PdOSn1 sol (see Section 2), has been frozen in liquid nitrogen and characterized by ¹¹⁹Sn Mössbauer spectroscopy. The frozen solution spectrum of a stannate solution at the same tin concentration as in the sol has also been recorded as a reference (see Fig. 4).

The difference between the spectra recorded for the Sn(OH)₆²⁻ solution and the bimetallic PdOSn1 sol is significant. An isomer shift close to zero is expected for the stannate solution because such a value, already reported in the literature [35], is typical of a symmetric environment in the coordination sphere of tin. In the bimetallic sol, the increase of both δ and Δ when compared to the stannate solution indicates a modification of the coordination sphere of tin (see Table 3). The increase of δ can be correlated to

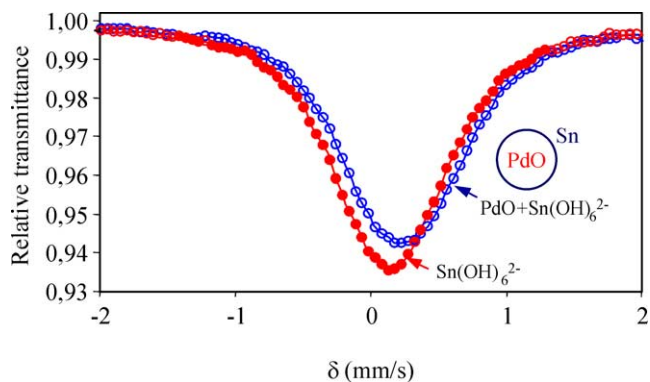
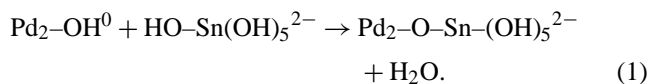


Fig. 4. ¹¹⁹Sn Mössbauer spectra at –193 °C of (●) the Sn(OH)₆²⁻ solution and of (○) the bimetallic PdOSn1 sol (PdO sol + Sn(OH)₆²⁻) at the same tin concentration ([Sn] = 1.3 × 10⁻² mol/L).

an increase of the electronic density of tin whereas that of Δ is related to a decrease in the symmetry of the close environment of tin. Hence, these results are consistent with the adsorption of Sn(OH)₆²⁻ complexes onto the PdO colloidal nanoparticles. Unfortunately, the Mössbauer spectrum of the PdOSn1 sol could not be decomposed into two contributions, the one related to adsorbed stannate and the other related to free stannate, because the corresponding hyperfine parameters were too close.

At pH close to 12, the surface of palladium oxide is negatively charged because of its point of zero charge: PZC(PdO) = 4.5 [21]. Therefore, electrostatic adsorption of the stannate anion to form an outer sphere complex [36] with the negatively charged PdO surface is not likely because of electrostatic repulsion. Using the multisite complexation model (MUSIC) [37,38], the different sites present at the surface of palladium oxide have been simulated in our previous study [25]. According to this model, in the investigated range of alkaline pH values, 2 surface hydroxyl groups are supposed to coexist, Pd₂–OH⁰ (μ 2 sites) and Pd₃–O^{-0.5} (μ 3 sites), yielding a negatively charged surface as expected. In this route, adsorption is suggested to proceed via chemisorption (hydrolytic adsorption) of stannate leading to the formation of an inner sphere complex [39] as described in



In this work, the influence of the preparation time of the PdOSn sol has been studied because we know from previous studies on Pd/Al₂O₃ catalysts prepared via colloidal oxide synthesis [25] that this parameter is crucial to control the state of aggregation of the supported palladium particles. In

Table 3

Hyperfine parameters of refined spectra of Sn(OH)₆²⁻ solution and PdOSn1 sol recorded at –193 °C

Sample	δ (mm/s)	Δ (mm/s)	Γ (mm/s)	RC (%)	Sn species
Sn(OH) ₆ ²⁻ solution	0.035 (4)	0.335 (7)	0.794 (8)	100	Sn ^{IV} symmetric environment
PdOSn sol	0.128 (3)	0.396 (6)	0.784 (8)	100	Sn ^{IV} distorted environment

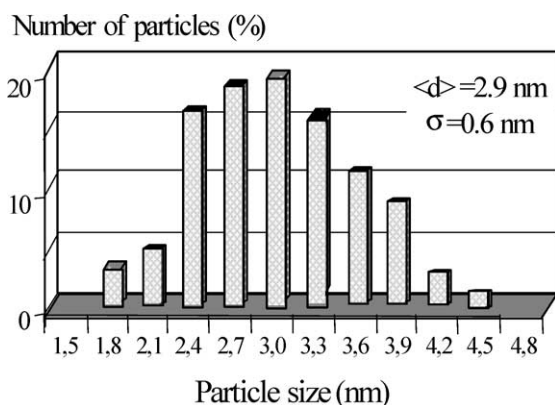
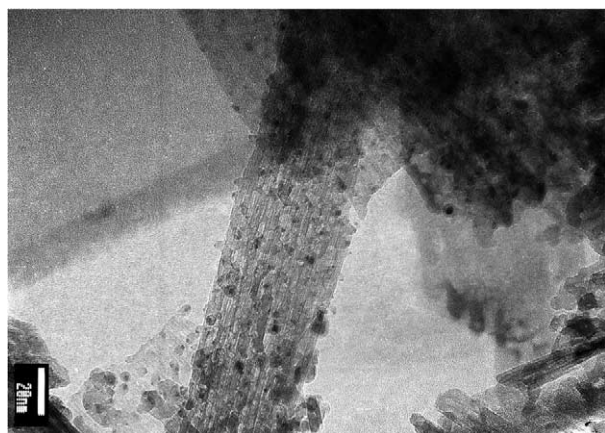


Fig. 5. TEM micrograph of the PdOSn1 catalyst and particle size distribution.

the PdOSn1 catalyst, the sol is immediately impregnated after its preparation while in the PdOSn2 catalyst, the sol is agitated 75 min before impregnation. A TEM micrograph and the particle size distribution of PdOSn1 are presented in Fig. 5. For this catalyst, only isolated supported particles have been observed. When compared to the starting PdO particles (mean particle size = 1.8 nm [25]), the mean particle size increases to 2.9 nm but the standard deviation of the distribution is kept the same.

For the PdOSn2 catalyst, together with isolated supported particles, three-dimensional aggregates of particles can also be observed by TEM (see Fig. 6). A similar particle size distribution with the same mean diameter as in PdOSn1 has been determined by analysis of the isolated particles of PdOSn2.

Concerning the state of aggregation of the supported particles, the difference between the PdOSn catalysts can be explained by taking into account the aggregation of the colloidal particles in the sol occurring with increasing preparation times. Indeed, it has been demonstrated in the monometallic case that the aggregation of the PdO colloidal particles occurs in the sol with time [25]. If the catalyst synthesis—including the preparation of the sol and deposition on the support—does not exceed a few minutes, aggregated PdO particles in the sol may be easily dispersed when contacted with the Al_2O_3 support. Under these con-

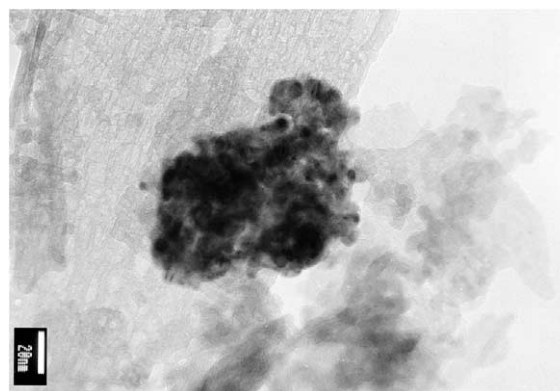


Fig. 6. TEM micrograph of an aggregate of particles on the PdOSn2 catalyst.

ditions, small aggregates (about 100 nm) of PdO particles in the sol are readily dispersed during wetness impregnation yielding a Pd/ Al_2O_3 catalyst with isolated supported palladium particles. On the other hand, for higher sol preparation times, three-dimensional aggregates whose size does not exceed 200 nm can be observed by TEM on the catalyst. In this case, the aggregates are not fully redispersed after impregnation on the support. To explain the irreversibility of this redispersion, it is proposed that weak interactions (e.g., van der Waals attractive forces) exist between PdO nanoparticles inside the aggregate when newly formed (small preparation time). These interactions are weak enough to be destabilized by the charged alumina surface during impregnation on the support. When the preparation time of the sol increases, the cohesion of the aggregates is strengthened by the formation of chemical bonds between the PdO particles. The redispersion of the aggregates by the support then becomes impossible. In the case of the bimetallic PdOSn catalysts, the aggregate of particles observed in the catalyst having the longer preparation time, PdOSn2, is suggested to proceed via the same kind of mechanism.

The difference in the state of aggregation of the supported particles of PdOSn1 and PdOSn2 implies pronounced differences in the formation upon reduction of the bimetallic Pd_xSn_y phases as demonstrated by the following ^{119}Sn Mössbauer spectroscopy study. The Mössbauer spectra are presented in Fig. 7 and Fig. 8, respectively for PdOSn1 and PdOSn2 and the corresponding hyperfine parameters are reported in Table 4.

For the PdOSn2 catalyst, a significant amount of Pd_2Sn alloy can be observed after reduction at 200 °C. By contrast, for the PdOSn1 catalyst, there is no bimetallic species under the same conditions. However, the reduction of tin is initiated as proven by the presence of 8% of Sn^{II} . For this catalyst, formation of bimetallic species starts at 300 °C and increases with the reduction temperature: 10% of PdSn at 300 °C and 49% of the expected Pd_2Sn alloy at 400 °C. In both catalysts, the molar Pd/Sn is 2. Hence, the maximum amount of Pd_2Sn observed approximately corresponds to 50% of alloyed palladium. Stannous tin is an intermediate species between stannic tin and reduced tin and acts as

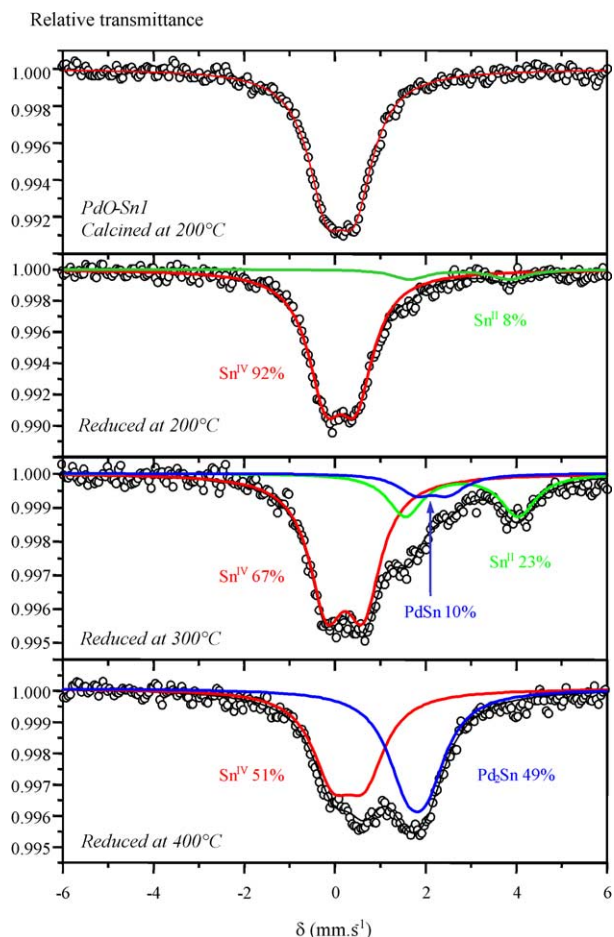


Fig. 7. ^{119}Sn Mössbauer spectra of the PdOSn1 catalyst calcined at 200 °C (top) and reduced at 200 °C, 300 °C, and 400 °C (bottom).

a precursor of the bimetallic Pd–Sn species. As Sn is not supposed to migrate easily on alumina because of the formation of tin aluminate [34], its incorporation into palladium demonstrates that the stannate anions adsorbed on the PdO particles in the sol remain in the vicinity of palladium after the deposition step of the sol onto the support. The increased mean particle size observed for the PdOSn catalysts could be explained by migration onto alumina of a part of the adsorbed stannate near the PdO particles.

The different behavior of the PdOSn catalysts toward bimetallic phase formation upon reduction is attributed to the different states of aggregation of their supported particles. It is suggested that tin is in stronger interaction with alumina for isolated supported particles. On the contrary, in the case of aggregates of particles, tin inside the aggregates does not interact with alumina and therefore forms bimetallic species under reducing atmosphere at lower temperature. For this reason, formation of Pd_xSn_y species in PdOSn1 (isolated particles) occurs at higher temperatures when compared to PdOSn2 (aggregates + isolated particles). In conclusion, the aggregated state of colloidal particles promotes the interaction between the two elements leading to the formation of an alloyed phase.

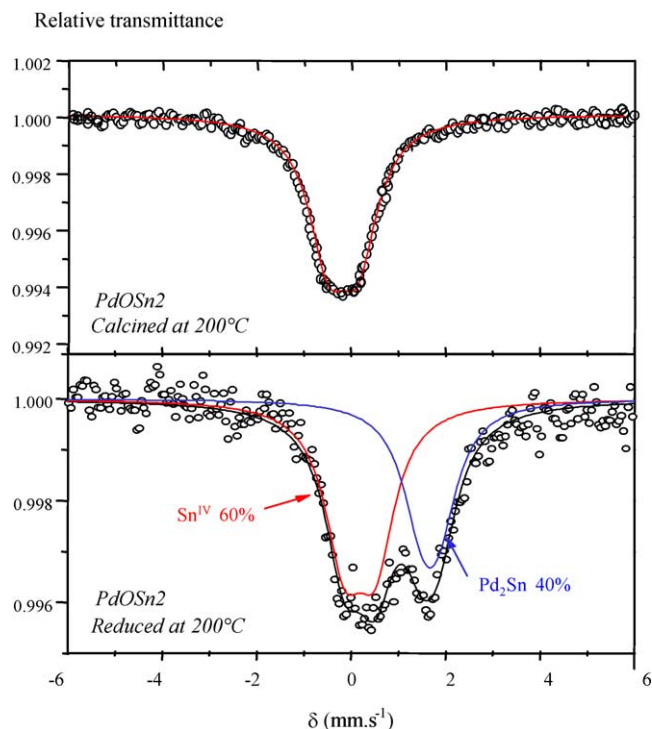


Fig. 8. ^{119}Sn Mössbauer spectra of the aggregated PdOSn2 catalyst after calcination (top) and reduction (bottom) at 200 °C.

Table 4

Hyperfine parameters of refined spectra of the PdOSn1 and PdOSn2 catalysts after calcination and reduction

Sample	δ (mm/s)	Δ (mm/s)	Γ (mm/s)	RC (%)	Sn species
PdOSn1 calcined at 200 °C	0.02 (1)	0.62 (1)	0.98 (2)	100	Sn^{IV}
PdOSn1 reduced at 200 °C	0.02 (1)	0.67 (1)	0.94 (2)	92	Sn^{IV}
	2.64 (9)	2.2 (1)	1.0 (2)	8	Sn^{II}
PdOSn1 reduced at 300 °C	0.12 (1)	0.80 (1)	0.94 (3)	67	Sn^{IV}
	2.05 (8)	0.7 (1)	0.94 (3)	10	PdSn
	2.69 (4)	2.49 (6)	0.94 (3)	23	Sn^{II}
PdOSn1 reduced at 400 °C	0.19 (2)	0.71 (3)	1.09 (4)	51	Sn^{IV}
	1.70 (3)	0.44 (5)	1.09 (4)	49	Pd_2Sn
PdOSn2 calcined at 200 °C	0.02 (1)	0.56 (1)	0.96 (2)	100	Sn^{IV}
PdOSn2 reduced at 200 °C	0.07 (3)	0.66 (3)	1.00 (6)	60	Sn^{IV}
	1.57 (4)	0.36 (8)	1.0 (2)	40	Pd_2Sn

4. Conclusion

In a conclusion, the chemistry of colloidal oxide provides powerful routes like surface precipitation and surface adsorption to prepare bimetallic supported catalysts in aqueous medium. By taking into account the specific reactivity of metallic cations in aqueous solution depending on pH or ligand effects, bimetallic colloidal particles can be obtained in the oxidized state as clearly demonstrated by ^{119}Sn Mössbauer spectroscopy for the adsorption of stannate anions onto PdO nanoparticles in the case of surface adsorption. For both routes, the interaction set at the colloidal state quantita-

tively evolves to the Pd–Sn bimetallic phase after activation of the alumina-supported catalysts. Initiating the interaction of Sn and Pd at the colloidal state considerably limits the interaction of tin with alumina on the supported catalyst explaining the significant formation of Pd_xSn_y phases for reduction temperatures as low as 200 °C.

In the case of surface adsorption, the extent of incorporation upon reduction of tin into palladium is suggested to be controlled by the aggregation state of the supported particles. For isolated particles (PdOSn1 catalyst), alloying starts at 300 °C whereas for aggregated particles (PdOSn2 catalyst) it occurs at 200 °C possibly because tin inside the aggregates does not interact any more with the alumina carrier. Therefore, the preparation time of the sol strongly influences the extent of aggregation of the colloidal particles and is the a key parameter for the preparation of the catalyst. For a short preparation time, isolated particles having narrow particle size distributions centered in the 2–3 nm range are obtained but formation of the Pd–Sn phase occurs at high temperatures. For a longer preparation time, alloying is observed at low temperatures but aggregates of particles are present on the catalyst. Thus, for an optimal preparation time, aggregation has started favoring alloying but its extent is limited to keep an acceptable metallic dispersion.

The influence of both the amount of Pd_xSn_y phase and the aggregation state of the supported particles on the catalytic properties in selective hydrogenation of buta-1,3-diene will be discussed in part II of this study for the catalysts prepared by surface adsorption [22]. In-depth surface characterization of the metallic particles will also be presented to illustrate relationships between the surface structure and the catalytic properties.

Acknowledgment

The authors thank Prof. J.P. Jolivet from Laboratoire de Chimie de la Matière Condensée (Université Pierre et Marie Curie, Paris, France) for fruitful discussions and interpretations of colloidal chemistry.

References

- [1] J. Barbier, in: E.H. Knözinger, J. Weitkamp (Eds.), *Handbook of Heterogeneous Catalysis*, Wiley–VCH, Weinheim, 1997, p. 257.
- [2] J.P. Candy, B. Didillon, E.L. Smith, T.M. Shay, J.M. Basset, *J. Mol. Catal.* 86 (1994) 179.
- [3] Y.A. Ryindin, Y.I. Yermakov, in: J.M. Basset, B.C. Gates, J.P. Candy, A. Choplin, M. Lecomte, F. Quignard, C. Santini (Eds.), *Surface Organometallic Chemistry: Molecular Approaches to Catalysis*, Kluwer, Dordrecht, 1988, p. 127.
- [4] J.L. Rousset, L. Stievano, F.J. Cadete Santos Aires, C. Geantet, A.J. Renouprez, M. Pellarin, *J. Catal.* 197 (2001) 335.
- [5] K. Esumi, M. Shiratori, H. Ishizuki, T. Tano, K. Torigoe, K. Meguro, *Langmuir* 7 (1991) 457.
- [6] H. Bönneeman, W. Brijoux, R. Brinkman, E. Dinjus, R. Fretzen, T. Jousen, B. Korall, *J. Mol. Catal.* 74 (1992) 323.
- [7] W. Vogel, P. Britz, H. Bönneeman, J. Rothe, J. Hormes, *J. Phys. Chem. B* 101 (1997) 11029.
- [8] D.G. Duff, T. Mallat, M. Schneider, A. Baiker, *Appl. Catal. A* 133 (1995) 133.
- [9] W. Yu, M. Liu, H. Liu, X. An, Z. Liu, X. Ma, *J. Mol. Catal. A* 142 (1999) 201.
- [10] Roucoux, Schulz, Patin, *Chem. Rev.* 102 (10) (2002) 3757.
- [11] N. Toshima, *J. Macromol. Sci. Chem. A* 27 (1990) 1225.
- [12] J. Belloni, M. Mostfalvi, H. Remita, J.L. Marignier, M.O. Delcourt, *New J. Chem.* 22 (1998) 1239.
- [13] R.S. Miner Jr., S. Namba, J. Turkevitch, *Stud. Surf. Sci. Catal.* 7 (1981) 160.
- [14] T. Yonezawa, N. Toshima, *J. Mol. Catal.* 83 (1993) 167.
- [15] A.F. Lee, C.J. Baddeley, C. Hardacre, R.M. Ormerod, R.M. Lambert, G. Schmid, H. West, *J. Phys. Chem.* 99 (1995) 6096.
- [16] C. Pan, F. Dassenoy, M.J. Casanove, K. Philippot, C. Amiens, P. Lecante, A. Mosset, B. Chaudret, *J. Phys. Chem. B* 103 (1999) 10098.
- [17] Y. Wang, N. Toshima, *J. Phys. Chem. B* 101 (1997) 5301.
- [18] M. Harada, K. Asakura, N. Toshima, *J. Phys. Chem.* 97 (1993) 5103.
- [19] N. Toshima, Y. Wang, *Langmuir* 10 (1994) 4574.
- [20] N. Toshima, P. Lu, *Chem. Lett.* 25 (8) (1996) 729.
- [21] B. Didillon, E. Merlen, T. Pagès, D. Uzio, *Stud. Surf. Sci. Catal.* 118 (1998) 41.
- [22] S. Verdier, B. Didillon, S. Morin, D. Uzio, *J. Catal.*, in press.
- [23] W. Künding, *Nucl. Inst. Methods* 75 (1969) 336.
- [24] L.I. Elding, L.F. Olsson, *J. Phys. Chem.* 82 (1978) 69.
- [25] T. Pagès, PhD thesis, University Paris VI, 1998.
- [26] S. Kratochvil, E. Matijevic, *Adv. Ceram. Mater.* 2 (1987) 798.
- [27] A. Garg, E. Matijevic, *J. Colloid Interface Sci.* 126 (1988) 243.
- [28] M. Ohmori, E. Matijevic, *J. Colloid Interface Sci.* 150 (1978) 594.
- [29] R.L. Cohen, K.W. West, *J. Electrochem. Soc.* 120 (4) (1973) 502.
- [30] D.K. Snediker, in: I.J. Gruverman, W. Seidel (Eds.), *Mössbauer Effect Methodology*, Vol. 2, 1966, p. 161.
- [31] R.P. Elliott, in: *Constitution of Binary Alloys*, 1st Supplement, McGraw–Hill, New York, 1986, p. 732.
- [32] E.A. Sales, J. Jove, M.J. Mendes, F. Bozon-Verduraz, *J. Catal.* 195 (2000) 88.
- [33] H. Berndt, I. Mönnich, B. Lücke, M. Menzel, *Appl. Catal. B* 30 (2001) 111.
- [34] T. Cholley, PhD thesis, University Paris VI, 1997.
- [35] G.M. Barvinok, S.R. Kasabyan, M.K. Khripun, M.M. Sychev, V.B. Lebedev, *J. Appl. Chem. USSR* 56 (1983) 1163.
- [36] J.P. Jolivet, in: *Metal Oxide Chemistry and Synthesis, from Solution to Solid State*, Wiley, New York, 2000, p. 285.
- [37] T. Hiemstra, W.H. van Riemsdijk, G.H. Bolt, *J. Colloid Interface Sci.* 133 (1989) 99, 105.
- [38] J.P. Jolivet, in: *Metal Oxide Chemistry and Synthesis, from Solution to Solid State*, Wiley, New York, 2000, p. 223.
- [39] J.P. Jolivet, in: *Metal Oxide Chemistry and Synthesis, from Solution to Solid State*, Wiley, New York, 2000, p. 286.